Journal of Computational Applied Mechanics 2022, 53(2): 190-203

DOI: 10.22059/JCAMECH.2022.342475.717

RESEARCH PAPER

Comparative study on the lateral stability strength of laminated composite and fiber-metal laminated I-shaped cross-section beams

Azadeh Soltani, Masoumeh Soltani*

Department of Civil Engineering, Faculty of Engineering, University of Kashan, Kashan, Iran

Abstract

The current investigation aims to peruse the discrepancies between the endurable transverse buckling load of multi-layer fibrous composite and fiber-metal laminate (FML) I-section beams. Using the energy method, the governing differential equations are extracted in accordance with the classical laminated plate theory and Vlasov's model for non-uniform torsion. Then, the equilibrium equations system is numerically solved via the differential quadrature method as a powerful and accurate technique, and finally, the lateral buckling load is calculated. Numerical results are presented for a simply supported I-beam under gradient moment. The accuracy of the proposed method is examined by comparing the results with those obtained by ANSYS finite element software. By considering the best conventional stacking sequences, the lateral stability strength of FML and laminated composite beams with I-shaped cross-sections are compared to each other for different fiber composite materials, end moment ratios, mode numbers, and metal volume fractions of the web and both flanges. The results show that the transverse buckling load of the selected I-beam is significantly affected by the mentioned parameters. In addition, the numerical outcomes indicate that the lateral buckling capacity of CARALL is more than GLARE for all analyzed cases.

Keywords: Lateral stability; Fiber metal laminates; Thin-wall beam; Conventional lay-ups; Differential quadrature method.

1. Introduction

Nowadays, due to the complexity of designing aerospace, marine and civil structures, and since fiber-reinforced epoxy composites have unique mechanical properties such as high fatigue resistance, durability, corrosion tolerance, and structural weight optimization, numerical and experimental research on laminated composite structural components have been rapidly expanded [1-40]. In this field, Rajasekaran and Nalinaa [41] assessed the vibrational characteristics and buckling behavior of non-prismatic composite spatial members having generic thin-walled section via the finite element method within the context of non-linear strain displacement relationship. Through a geometrically non-linear theory and employing the assumptions of large displacements and rotations, Machado and Cortinez [42] studied the free vibrational response of composite beams with doubly-symmetric thin-walled open cross-section loaded by arbitrary external forces. By the help of the finite element methodology, the flexural-

* Corresponding author. Tel.: +98-31-55912412; fax: +98-31-55912424.
E-mail address: msoltani@kashanu.ac.ir

torsional coupled free vibrational behavior and buckling problem of thin-walled composite beams were precisely investigated by Vo and Lee [43] considering the impacts axial load on the vibration characteristics. Based on linear fracture mechanics and Castigliano theory, the influence of edge crack ratio and its position on free vibration responses and lateral buckling strength of laminated composite slender beam was carried out by Karaagac et al. [44]. To estimate the buckling resistance of simply supported thin-walled structural members made of Fiber Reinforced Polymer (FRP) loaded by axially and uniformly transverse forces, Ascione et al. [45] developed a mechanical model on the basis of the assumptions of small strains and moderate rotations. In the contex of different patterns of beam's model, the mechanical characteristics involving the vibrational response and stability strength of laminated composite members subjected to different loading cases and end conditions were completely studied in Refs. [46-49]. Through a one dimensional finite element model, Asadi et al. [50] analyzed the linear stability behavior of laminated composite beams with thin-walled open/closed sections subjected various boundary conditions. In their study, the impacts of transverse shear deformation and out-of-plane warping of the beam section are taken into consideration. Moreover, different numerical and analytical studies on the static and dynamic analyses of composite structural elements with different shapes and geometries exposed to various external loadings are presented in Refs. [51, 52].

Fiber-metal laminates (FMLs) are a hybrid multilayer composed of thin metal sheets and fiber-reinforced composite plies and are prepared by bonding fibers and resins in layers. FMLs have the simultaneous advantages of both fiber polymer composites and metals. In this regard, most of existing literature on the behavior FMLs mechanical elements is focused on cylindrical shells [52-56]. In addition, Dhaliwal et al. [57], via a laboratory study, investigated the behavior of fiber-metal multilayers by adding resin under an impact force and reported that adding resin between the layers results in decreasing the separation by 40-50% and increasing the compressive strength by approximately 30%. Mohandes et al. [58] extracted the equations governing the free vibration of the cylindrical shell made of metal-fiber composite layers based on the first-order shear deformation theory. Their work evaluated various parameters such as different material properties of composite fibers, lay-up arrangement, fiber angle, boundary conditions, number of vibrational modes, and metal volume fraction (MVF). In addition, Mania et al. [59] and Banat et al. [60, 61] evaluated the flexural buckling and post-buckling behavior of FMLs composite thin-walled beams with C- and Z-shaped sections under axial compressive force via both numerical and experimental studies.

Owing to hybrid composite thin-walled beams applications in aircraft and spacecraft structures, wind turbines, and helicopter blades, it is essential to provide an accurate numerical and/or analytical solutions along with the possible modeling in a commercial finite element software to estimate the stability resistance of these structures. Motivated by this fact, lateral-torsional buckling of a multi-layer thin-walled beam with a symmetrical cross-section made of fiber-metal composites under externally transversely loading is investigated in this study. For this purpose, and as the first step, stability equations of thin-walled members are extracted via Vlasov's model, the classical laminated plate theory (CLPT), and the energy method. Then, the differential quadrature method (DQM) is employed to discretize and solve the governing equations. Next, to examine the obtained results' accuracy and reliability, they are compared with those acquired from modeling in ANSYS finite element software, and a good agreement is observed between them. Lastly, the effect of important parameters such as end moment coefficient, MVF, mode number, and material type of fiber on the stability behavior of the pre-specified multi-layer hybrid composite I-beam having the conventional angle-ply and unidirectional layups for the web and the flanges is investigate. In addition, the lateral buckling resistance of FML and laminated composite I-section beam with uniform cross-section are compared through an exhaustive parameterization study. The numerical results of this research can be considered as a reference for future computational validation of the lateral stability strength of FML thin-walled beams.

2. Fundamental equations

Figure 1 shows the schematic representation of transversely loaded FML I-section member of length span L. The height of the web and the width of both flanges are assumed d and b, respectively. As presented in Fig. 1b, all section walls of the considered I-section bam consist of two metal sheets at the outer sides of fiber reinforced epoxy composite layers. $(t_w)_k$ is the thickness of the web ply and t_w is the overall thickness of the web section. $(t_f)_k$ is the thickness of each ply of the flanges and t_f is thus the total thicknesses of each flanges. In Fig. 1d, x, and y, z are utilized coordinates along the length and two plannar directions. The coordinate components are measured from the centroid of the I-shaped cross-section. Also, u_0, w_0 and v_0 are the axial displacement, the transverse deflection along the z-axis, and the lateral displacement component in the y-direction. ϕ_x represents the rotation of the I-shaped cross-section about x-axis and is commonly called the twisting angle.

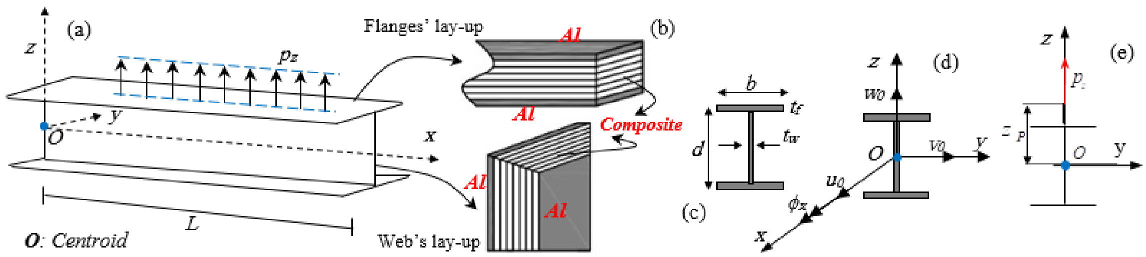

Fig 1: (a) Configuration for transversely loaded FML beam with an I-shaped cross-section, (b) Lamination stacking sequences of the web and both flanges, (c) Geometry properties, (d) Coordinate system, notation for displacement parameters, (e) Definition of load eccentricities.

For a laminated composite structure consists of N_L perfectly bonded orthotropic layers, the stiffness quantities including A_{ij} , B_{ij} and D_{ij}, which are the extensional, coupling and the bending stiffness matrix, respectively, are generally presented on the basis of the transformed reduced stiffness (Q_{ij}^f and Q_{ij}^w $(i = j = 1,\ 6)$) as what follows [46]:

$$(A_{ij}^f, B_{ij}^f, D_{ij}^f) = \sum_{k=1}^{N_L}\int_{z_k}^{z_{k+1}} (Q_{ij}^f)_k (1, z, z^2)dz\,,\ (A_{ij}^w, B_{ij}^w, D_{ij}^w) = \sum_{k=1}^{N_L}\int_{y_k}^{y_{k+1}} (Q_{ij}^w)_k (1, y, y^2)dy\,. \tag{1}$$

Here, the superscripts $(\bullet)^w$ and $(\bullet)^f$ are adopted to exhibit the wall sections including the web and flanges. In addition, z_k and z_{k+1} are the distances of outer and inner surfaces of the k_{th} layer with respect to the mid-plane of thickness in the flanges, respectively. Also, y_k and y_{k+1} refer to the web lamina distances of outer and inner surfaces of the k_{th} layer with respect to the mid-line of thickness, respectively. For symmetrically balanced laminates I-shaped cross-sections consisting of two equal flanges and one web, the cross-sectional rigidity components including, the axial rigidity of the FML I-shaped section ($\overline{EA}$), the flexural rigidities about the y- and z directions ($\overline{EI}_y$, $\overline{EI}_z$), additionally, the St-Venant torsional rigidity relating to uniform torsion ($\overline{GJ}$), as well as, the warping rigidity for non-uniform torsion ($\overline{EI}_\omega$), are described by the following equations [43]:

$$\begin{aligned}&\overline{EA} = 2bA_{11}^f + dA_{11}^w,\ \overline{EI}_y = 2bD_{11}^f + \frac{d^2}{2}bA_{11}^f + \frac{d^3}{12}A_{11}^w,\ \overline{EI}_z = \frac{b^3}{6}A_{11}^f + dD_{11}^w,\\ &\overline{EI}_\omega = (\frac{d^2}{4}A_{11}^f + D_{11}^f)\frac{b^3}{6} + \frac{d^3}{12}D_{11}^w,\ \overline{GJ} = 4(2bD_{66}^f + dD_{66}^w).\end{aligned} \tag{2}$$

Based on these assumptions, and according to Vlasov's theory [62], the weak statement of equilibrium equations of the selected FML I-shaped cross-section beam initially loaded by the transversely distributed force in the z-direction (p_z) can be represented as [39, 63]:

$$\begin{aligned}&\delta\Pi = \int_0^L \left(\overline{EA}u_0'\delta u_0' + \overline{EI}_y w_0''\delta w_0'' + \overline{EI}_z v_0''\delta v_0'' + \overline{EI}_\omega \phi_x''\delta\phi_x'' + \overline{GJ}\phi_x\delta\phi_x'\right)dx\\ &-\int_0^L \left(M_y^0(x)v_0''\delta\phi_x + M_y^0(x)\phi_x\delta v_0''\right)dx - \int_0^L \left(p_z(x)z_P\phi_x\delta\phi_x\right)dx = 0\end{aligned} \tag{3}$$

Here, z_P represents the vertical distance between the point of application of the arbitrary transverse force $p_z(x)$ and the centroid, which is commonly called the load height parameter (Fig. 1e). Additionally, the parameter $M^0(x)$ is the pre-buckling bending moment loading with respect to the y-axis.

By gathering the coefficients of the virtual displacements ($\delta u_0, \delta v_0, \delta w_0, \delta\phi_x$), and after equating them to zero, the system of equilibrium equations for FML I-section beam under transverse loading is extracted as what follows:

$$\overline{EA}u_0'' = 0 \tag{4}$$

$$\overline{EI}_y w_0^{IV} = p_z(x) \tag{5}$$

$$\overline{EI}_z v_0^{IV} - (M_y^0(x)\phi_x)'' = 0 \tag{6}$$

$$\overline{\mathrm{EI}}_\omega \phi_x^{IV} - \overline{GJ}\phi_x'' - M_y^0(x) v_0'' + p_z(x) z_P \phi_x = 0 \tag{7}$$

Through the minimum potential energy principle, the subsequent boundary conditions at x=0 and x=L are also determined:

$$\begin{aligned}
&\overline{EA}u_0' = 0 && \text{or} && \delta u_0 = 0\\
&\overline{EI}_y w_0'' = 0 && \text{or} && \delta w_0' = 0\\
&\overline{EI}_y w_0''' = 0 && \text{or} && \delta w_0 = 0\\
&\overline{EI}_z v_0'' = 0 && \text{or} && \delta v_0' = 0\\
&\overline{EI}_z v_0''' - (M_y^0 \phi_x)' = 0 && \text{or} && \delta v_0 = 0\\
&\overline{EI}_\omega \phi_x'' = 0 && \text{or} && \delta \phi_x' = 0\\
&\overline{EI}_\omega \phi_x''' - M_y^0 v_0' = 0 && \text{or} && \delta \phi_x = 0
\end{aligned} \tag{8}$$

Since the current study is concerned with stability analysis of a transversely loaded FML I-section beam, the first two equilibrium equations (Eqs. (4) and (5)) have no involvement in assessing lateral buckling capacity of the considered member. While to peruse the lateral buckling, the two-coupled differential equations in terms of the lateral displacement and the torsion angle (Eqs. (6) and (7)) should be considered.

3. Solution Methodology

In this section, the numerical solution of the resulting coupled differential equations is developed. The Generalized Differential Quadrature Method (GDQM) is employed for this purpose and to calculate the axial critical loads. This methodology is based on the approximation of a derivative of a function at a specified point by the sum of the weighted factors and the values of the function at any set points in the problem solving range. According to GDQM, the m^{th} order derivative of a function *f(x)* at an arbitrary point is described as [64]

$$\frac{d^m f(x_i)}{dx^m} = \sum_{j=1}^{N} C_{ij}^{(m)} f(x_j) \quad for \quad i = 1, 2, ..., N \tag{9}$$

where N is the number of grid points along x direction. x_j signifies the position of each sample point and $f(x_j)$ is function values at grid points x_j (i = 1, 2, …, N). Moreover, $C_{ij}^{(m)}$ denotes the weighting coefficient for the m^{th}-order derivative and is computed by the following algebraic formulations:

$$C_{ij}^{(1)}=\begin{cases}\dfrac{M(x_i)}{(x_i-x_j)M(x_j)} \quad for \quad \mathrm{i}\neq \mathrm{j} \\ -\sum\limits_{k=1,k\neq i}^{N} C_{ik}^{(1)} \qquad for \quad \mathrm{i{=}j} \\ M(x_i)=\prod\limits_{j=1,j\neq i}^{N}(x_i-x_j) \quad for\ i=1,2,...,N\end{cases} \quad i,j=1,2,...,N \quad ;\ C_{ij}^{(m)}=C_{ij}^{(1)}C_{ij}^{(m-1)} \qquad 2\le m\le N-1. \tag{10}$$

In this study, Chebyshev–Gauss–Lobatto approach is used to define the position of each sample point [65]

$$x_i=\frac{L}{2}\left[1-\cos\left(\frac{(i-1)\pi}{(N-1)}\right)\right],\ \ i=1,2,...,N\ . \tag{11}$$

Within the frame of the GDQM, the general form of the solution of two-coupled differential equations for the lateral displacement and the twisting angle can be expressed in the form of the following matrix:

$$\left[H\right]_{2N\times 2N}\left\{V^*,\ \phi^*\right\}_{2N\times 1}^{T}=\left\{0,\ 0\right\}_{2N\times 1}^{T} \tag{12}$$

Where

$$\begin{aligned}&H_{11}=\left[a^1\right]\left[C\right]^{(4)},\ H_{12}=\left[b^1\right]\left[C\right]^{(2)}+\left[c^1\right]\left[C\right]^{(1)}+\left[d^1\right],\\ &H_{21}=\left[d^2\right]\left[C\right]^{(2)},H_{22}=\left[a^2\right]\left[C\right]^{(4)}+\left[b^2\right]\left[C\right]^{(2)}+\left[c^2\right],\\ &\left\{V^*\right\}_{N\times 1}=\left\{v_0(\varsigma_1)\quad v_0(\varsigma_2)\quad ...\quad v_0(\varsigma_N)\right\}^T,\left\{\phi^*\right\}_{N\times 1}=\left\{\phi_x(\varsigma_1)\quad \phi_x(\varsigma_2)\quad ...\quad \phi_x(\varsigma_N)\right\}^T.\end{aligned} \tag{13}$$

in which

$$\begin{aligned}&a_{jk}^1=(\overline{EI_z})\delta_{jk},\ b_{jk}^1=-(L^2M_y^0\big|_{\varsigma=\varsigma_j})\delta_{jk},\ c_{jk}^1=-(2L^2M_y^{0\prime}\big|_{\varsigma=\varsigma_j})\delta_{jk},\ d_{jk}^1=-(L^2M_y^{0\prime\prime}\big|_{\varsigma=\varsigma_j})\delta_{jk},\\ &a_{jk}^2=(\overline{\mathrm{E}I_\omega})\delta_{jk},\ b_{jk}^2=-(L^2\overline{GJ})\delta_{jk},\ c_{jk}^2=(L^4p_z z_P\big|_{\varsigma=\varsigma_j})\delta_{jk},\ d_{jk}^2=-(L^2M_y^0\big|_{\varsigma=\varsigma_j})\delta_{jk}.\end{aligned} \tag{14}$$

Here, ζ is the non-dimensional form of the longitudinal variable (x) and describes as $\zeta=x/L$. It is necessary to point out that the afore-mentioned parameter (ζ) is adopted to facilitate the mathematical procedure via applying the DQM. After the implementation of the corresponding end conditions of transversely loaded FML beam with an I-shaped section, the lateral buckling resistance is eventually computed from the eigenvalue solutions of Eq. (12). To this aim, the endurable transverse critical load is obtained by zeroing the determinant of matrix $[H]_{2N\times 2N}$.

4. Numerical results and discussion

The lateral-torsional stability differential equations of I-section beams were obtained based on the CLPT and Vlasov's model in the previous sections. Then, to determine the lateral buckling load, the GDQM was employed. In the following example, a simply-supported thin-walled member under a variable bending moment (M_0, ηM_0), as shown in Fig. 2, is considered. All section walls (one web and two flanges) of composite multi-layer I-section beam are separately composed of two outer 2024-T3 Aluminium layers with six inner-plies of fiber composite. In the present study, the inner fiber-reinforce plies can be made from carbon-epoxy (CARALL) or glass-epoxy (GLARE) with the mechanical properties listed in Table 1. It should be noted that in this example, the thicknesses of both flanges and web are the same.

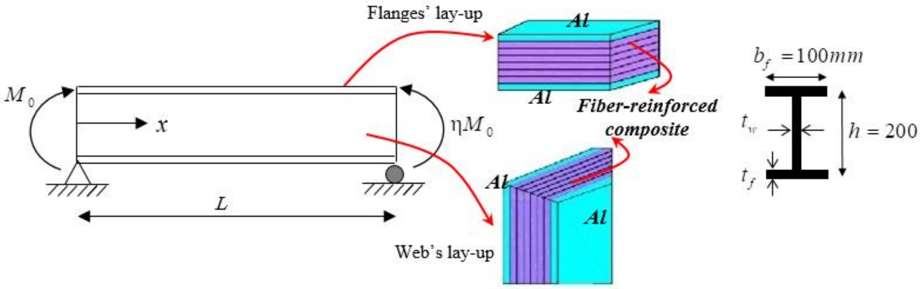

Fig 2: FML I-shaped beam exposed to end bending moment: wall section arrangement, and geometric data.

Table 1: Mechanical properties of the materials [55]

Property	E_1(GPa)	$E_2 = E_3$(GPa)	$G_{12} = G_{13}$(GPa)	$\upsilon_{12} = \upsilon_{13}$
Carbon/Epoxy	181	10.3	10.17	0.28
Glass/Epoxy	38.6	8.27	4.14	0.26
Al 2027-T3	72.4	72.4	27.2	0.33

In this section, after confirming the validity of the results, the lateral buckling resistance of laminated composite and FML I-shaped beam is compared considering the effect of various parameters such as, end moment ratio, MVFs of the web and bot flanges, mode number, and fibers material type. MVF is a dimensionless parameter that is defined by the following expression [52]:

$$MVF = {(k \times t_{Al})}\big/{t_{Lam}} \tag{15}$$

In this formula, k denotes the Aluminium layers number, t_{Al} and t_{Lam} are each Aluminium sheet thickness and the total lamina thickness, respectively. Furthermore, MVF equating zero means that there are just polymer fiber composite layers and if MVF equates 1, it means that all layers are metal.

4.1. Verification

Since the present model has not been investigated up-to-date by other researchers, there is no comparable result in the available literature. Therefore, to evaluate the accuracy and validity of the proposed method, the critical buckling moment of the simply supported thin-walled FML beam is obtained in which the structure is made of orthotropic fibers of glass-epoxy and carbon-epoxy with cross-ply arrangement $[Al, 0, 90, 0]_S$ and MVF=0.25 for 21 nodes across the longitudinal direction (N), and is compared with the results of modelling in ANSYS software in terms of end moment coefficient in Fig. 3.

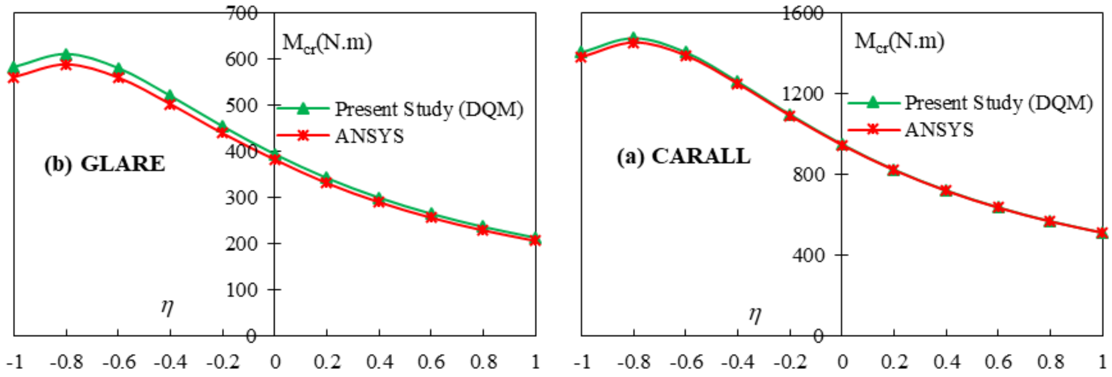

Fig 3: Variation of buckling moment of FML beam having I-shaped cross-section subjected to gradient bending moment with respect to the end moment ratio η: (a) CARALL section, (b) GLARE section.

Based on Fig. 3, it can be concluded that the present study results are accurate compared to those obtained by ANSYS, and for all values (η) error percentage is less than 3.

It should be noted that the Shell281 element in ANSYS simulate the laminated composite thin-walled beam.

Shell281 element has eight nodes, and each one has six degrees of freedom (DOF) (three DOF for displacement in x, y, z directions; and three DOF for rotation about x, y, z axes), that is appropriate for analysing thin or moderately-thick members [66]. In all simulated ANSYS models, the applied aspect ratio of the mesh (length-to-maximum width) was close to unity through the beam length (Fig. 4a). It is necessary to note that the delamination between the fiber composite and Aluminium layers is neglected in the formula presented herein, and a continuous construction is supposed. As a result, in 3D modelling using ANSYS software, the above-mentioned assumption has been considered, and consequently, a complete linking and connection between the fiber composite layers and metal face-sheets have been used. It is also assumed that the shear flow is completely transferred from the flanges to the web, and thus, in 3D modelling of the joint node at the junction border between the flanges and web has been adopted. In this regards, Fig. 4b shows the overall lateral-torsional buckling mode shape of the selected GLARE beam subjected to pure bending. In the finite element method (FEM) models, local buckling of the web and both flanges is not evident.

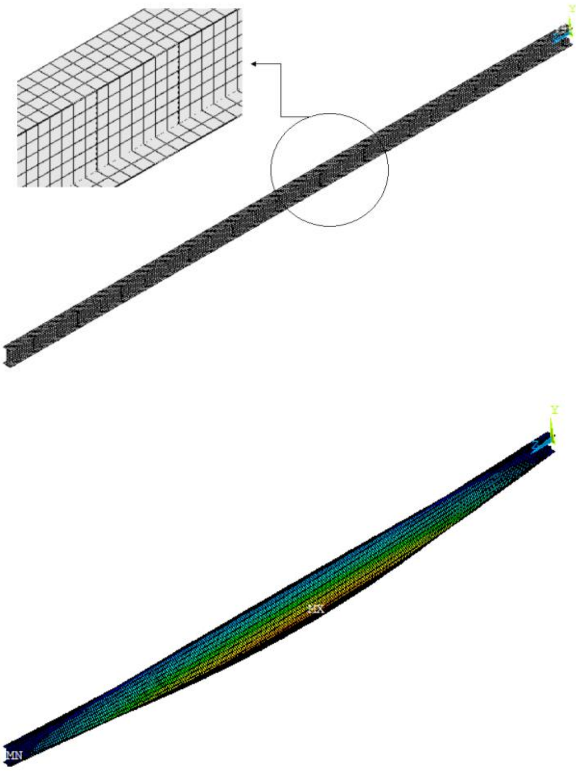

Fig 4: (a) View of mapped mesh used for the selected beam element under pure bending using ANSYS, (b) the FEM result using ANSYS for the first lateral-torsional buckling mode shape.

4.2. Comparison between buckling moment of FML and composite I-section beam

The aim of this subdivision is to precisely examine the impact of MVF, the value of η, buckling mode number, and fiber composite materials on the lateral-torsional stability capacity of the contemplated beam with an I-shaped cross-section exposed to the gradient bending load. Referring to the authors' knowledge, the best typical and practical lay-up arrangements for acquiring the highest lateral buckling load is attained by aligning the fiber of both flanges at zero degree through the longitudinal direction, and placing the web's fiber at an angle of ±45 between two Aluminium sheets [63, 67]. This statement can be expected regarding Eq. (2), because the values of flexural stiffness $\overline{EI}_z$ as well as warping stiffness $\overline{EI}_\omega$ are expressed in terms of unidirectional stiffness parameters (A_{11}^f, A_{11}^w and D_{11}^f, D_{11}^w). These two components reach their maximum magnitudes when the fibers that construct both flanges and the web are aligned in the longitudinal direction with a zero angle. Since the flanges have the responsibility of withstanding the flexural and torsional moments, to increase the lateral-torsional stability capacity, the flange fibers should be arranged in one direction with a zero-degree angle. Also, according to Eq. (2), the expression of St-Venant's torsional rigidity $\overline{GJ}$ depends on torsional stiffness components (D_{66}^f , D_{66}^w) in both flanges and the web of the cross-section. These two parameters usually reach their maximum values by placing the fibers of the composite layers in direction of ±45°. Because the beam web withstands shear stresses and has the task of transmitting shear force, the fiber layers of the web must be placed at an angle of ±45° to achieve the maximum shear capacity. Motivated by these facts, the most appropriate practical lay-up arrangements of both the flanges $[Al,(0)_3]_S$ and the web $[Al,(45)_3]_S$ is contemplated in the continuation. In this regard, the selected I-section beams with FML hybrid structure of (glass-epoxy or carbon-epoxy) with two outer Aluminium layers, as shown in Fig. 2, are analysed. For this purpose, the 1st buckling moment variations in terms of end moment coefficient (η) have been perused, in which the Aluminium volume fraction increases at each step, and the results for both material fibers are presented in Fig. 5. Similarly, the impact of volume fraction parameter on the variation of the 2nd buckling moment of simply supported I-shaped beams with respect to end moment ratio (η) for two different fibrous materials (glass/epoxy and carbon/epoxy) is given in Fig. 6.

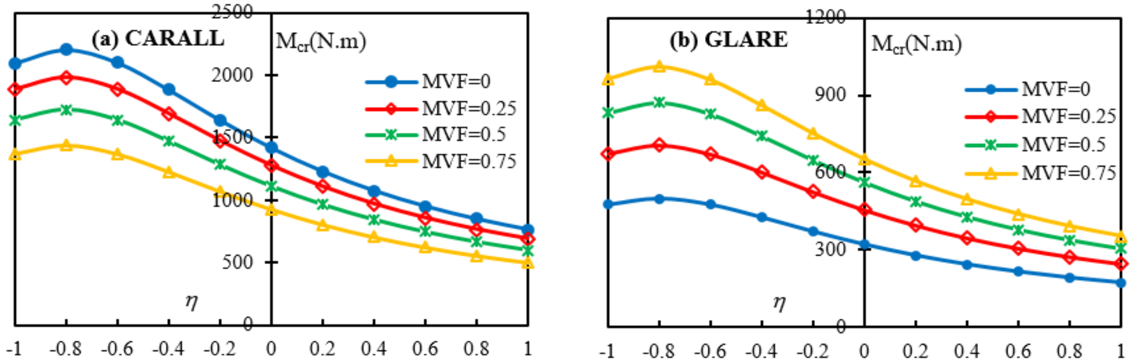

Fig 5: Variation of the lowest buckling moment of FML beam having I-shaped cross-section subjected to gradient bending moment with respect to η and for four different MVFs: (a) CARALL section, (b) GLARE section.

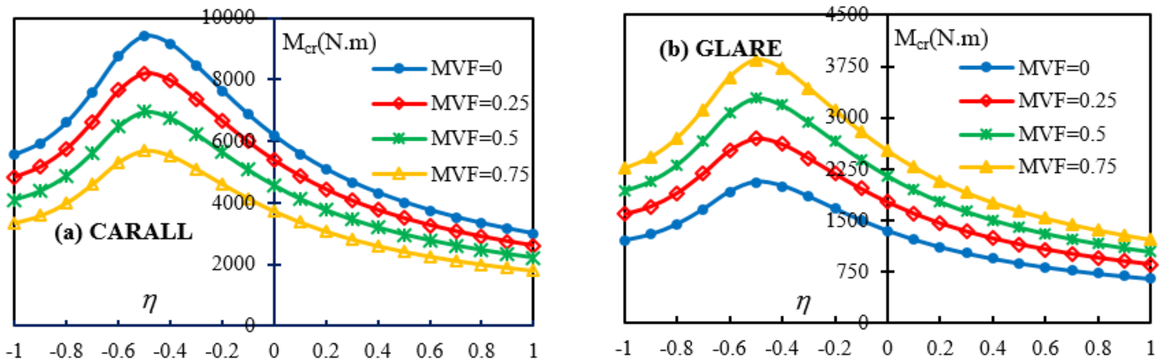

Fig 6: Variation of the 2nd buckling moment of FML beam having I-shaped cross-section subjected to gradient bending moment with respect to η and for four different MVFs: (a) CARALL section, (b) GLARE section.

In the following, the magnitude of first two buckling moments (M_{cr}) for various values of end moment ratios (η) with three different Aluminium volume fractions (MVF=0.3, 0.6 and 0.9) are tabulated in Table 2. Two types of FML are considered: GLARE and CARALL I-shaped beams with constant cross-section.

Table 2: The first two buckling moments (M_{cr}) for FML I-beam with different materials and subjected to different gradient moments.

Material	η	The first buckling moment (N.m)			The second buckling moment (N.m)		
		MVF=0.3	MVF=0.6	MVF=0.9	MVF=0.3	MVF=0.6	MVF=0.9
GLARE	+1	258.912	324.572	379.673	895.123	1115.107	1322.841
	+0.8	287.365	360.238	421.398	995.325	1239.934	1470.923
	+0.6	321.858	403.473	471.989	1123.015	1399.003	1659.630
	+0.4	364.011	456.297	533.827	1291.578	1608.981	1908.752
	+0.2	415.645	520.986	609.600	1522.543	1896.660	2250.145
	0	478.300	599.453	701.590	1845.979	2299.407	2728.381

	-0.2	551.918	691.609	809.730	2279.719	2839.286	3370.022
	-0.4	632.085	791.945	927.520	2732.759	3403.471	4039.806
	-0.6	705.209	883.537	1034.857	2634.441	3282.769	3891.959
	-0.8	741.984	929.804	1088.546	1981.642	2468.937	2928.110
	-1	707.607	886.882	1037.889	1659.301	2066.942	2452.375
	+1	672.308	560.957	438.822	2528.385	2047.696	1555.922
	+0.8	746.226	622.622	487.053	2811.419	2276.921	1730.096
	+0.6	835.960	697.449	545.550	3172.125	2569.048	1952.059
	+0.4	945.858	789.022	617.085	3648.456	2954.778	2245.108
	+0.2	1080.927	901.444	704.805	4301.921	3483.753	2646.815
CARALL	0	1245.595	1038.290	811.409	5219.866	4226.090	3209.941
	-0.2	1440.088	1199.636	936.871	6456.570	5224.720	3966.271
	-0.4	1652.384	1375.614	1073.599	7740.262	6263.487	4754.706
	-0.6	1844.099	1535.077	1197.926	7415.370	6012.790	4574.297
	-0.8	1935.221	1612.354	1259.368	5589.167	4528.820	3442.935
	-1	1841.615	1535.456	1200.196	4690.693	3797.923	2885.004

The next part investigates precisely the effect of increasing the metal volume fraction on the lateral-torsional buckling capacity. Again, the beam with a more appropriate lay-up configurations of carbon-epoxy (CARALL) and glass-epoxy (GLARE), which mentioned earlier, is considered. The variation of the critical lateral moment, for varying values of MVF, ranging from 0.0 to 1, is presented in Fig. 7 under the assumption of η =-1, 0, and 1 (end moment ratio).

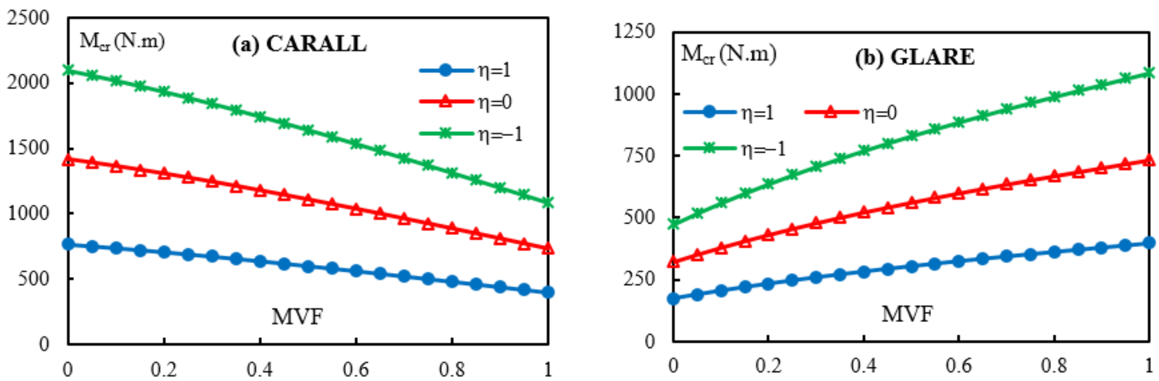

Fig 7: Variation of buckling moment of FML beam having I-shaped cross-section subjected to gradient bending moment with respect to MVF and for three different end moment parameters (η): (a) CARALL section, (b) GLARE section.

As shown in Figs. 5-7, the buckling moment capacity for all values of the end moment coefficient for an FML hybrid beam consisting of six layers of glass-epoxy increases significantly by enhancing the Aluminium volume fraction percentage. Whereas, in the case of CARALL, the opposite trend is observed. This decreasing pattern can be observed for the first two buckling moments. It means that increasing the MVF leads to a reduction in the value of the critical bending moment of CARALL I-beam. For the loading case considered in this example (Fig. 5), the first buckling moment for a prismatic GLARE I-shape member under pure bending (η=1) enhances by about 34%, when the metal percentage increases from 0 to 20%. As may be seen in the case of CARALL uniform I-beam exposed to pure bending, the volume fraction Aluminium equals MVF=0.2 reduces the magnitude of the buckling moment by about 7.67% compared to the conditions without two metal face-sheets (MVF=0). Also, according to Figs. 5 to 7 and Table 2, it can be seen that CARALL sections always have more lateral stability capacity. Since the elastic material characteristics and the modulus of elasticity of carbon/epoxy are more than glass/epoxy (Table 1), this outcome is expectable. For both CARALL and GLARE thin-walled laminated I-beams and different MVFs (Figs. 5 and 6), the variation of the beam lateral stability strength with η for different buckling modes is non-linear. As presented by these illustrations, it can be found that the most stable state against the 1st buckling moment for all the cases analysed occurs at η=-0.8, and, as expected, the most unstable condition occurs under the pure bending (η=1). Additionally, the maximum second buckling moment is obtained for η=-0.5. These outcomes concord with the previous results presented for homogenous beams with an I-shaped cross-section [68].

Subsequently, Fig. 8 illustrates the variation of the lowest buckling moments with respect to the aluminium percentage in the web and the flanges by setting the end moment parameter (η) equals -0.8.

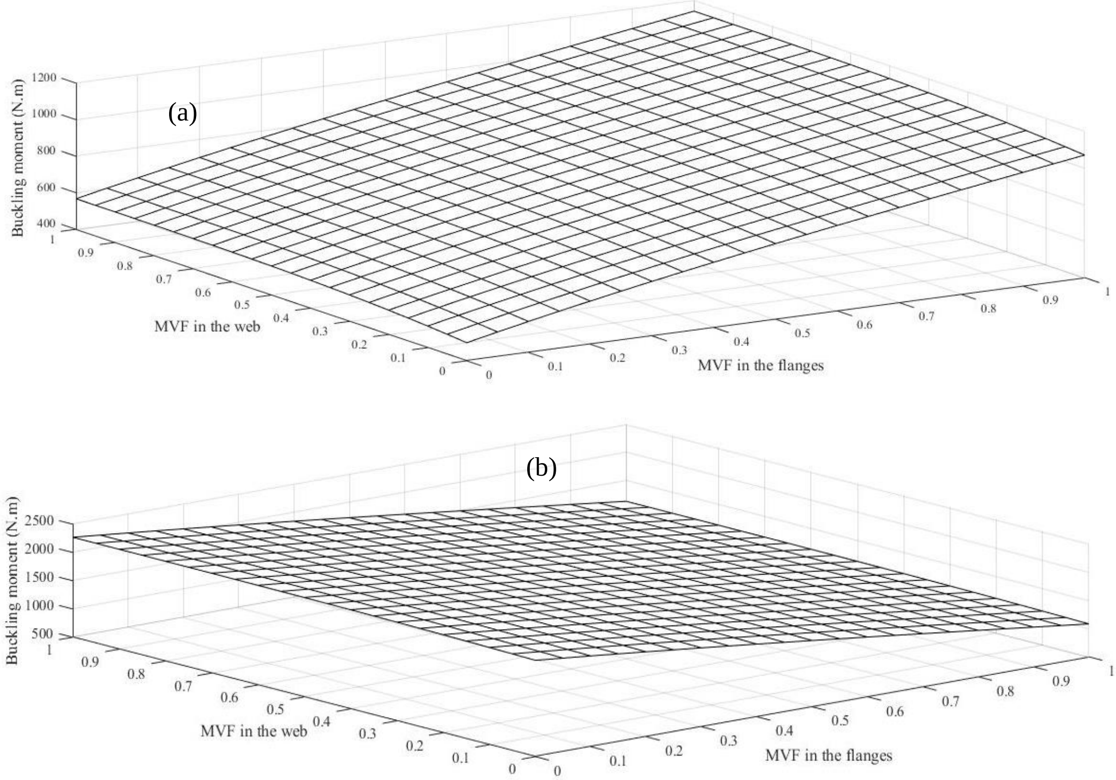

Fig 8: Variation of buckling moment of fiber-metal laminated beam with constant I-section for different web and flange MVFs: (a) GLARE, (b) CARALL.

From these graphical representations, it is again found that the values of MVF of the web and both flanges have a remarkable influence on the lateral stability strength of simply supported FML I-section beams exposed to gradient bending moment. It is easily recognized that the critical moment of GLARE beams with I-shaped cross-section increases with an increase in the metal percentages of the web and/or flanges, as a result of the enhancement of all stiffness quantities of the elastic member including the flexural and torsional rigidities. In contrast to GLARE beam, the critical moment of CARALL member with carbon-epoxy inner layers diminishes when the flanges' MVF is increased from 0 to 1, but with increasing the Aluminium percentage of the web, this pattern is converted. In addition, it can be stated that this interesting phenomenon is negligible on the lateral buckling capacity of CARALL I-section beams by the simultaneous increment of MVF in all section walls. Finally, it is obvious that the influence of the percentage of metal in both flanges on the value of buckling moments is more predominant than that of MVF of the web. The reason is attributed to the fact that the lateral-torsional instability mode occurs about the minor moment of the inertia axis.

5. Conclusions

In this work, the endurable lateral buckling loads of FML and laminated composite beams with an I-shaped cross-section under transverse loadings are compared to each other. Initially, the two-coupled fourth-order stability differential equations in terms of the lateral displacement and the twisting angle were derived according to Vlasov's model along with the CLPT. Then, differential equations were discretized using the GDQ numerical approach, and the lateral buckling load was calculated. After verifying the correctness of the results, the lateral stability strength of FML and laminated composite beams with I-shaped cross-sections having the conventional lay-up sequences are contrasted through various parameters such as composite material, end moment ratio, mode number, and metal volume fractions of the web and both flanges. After reviewing the numerical examples, the following significant findings are expressed below:

- It can be obtained that the most stable condition against lateral-torsional buckling for all the analysed cases occurs at η=-0.8 and, as expected, the most unstable condition occurs in the pure bending condition (η=1).
- The results indicated that for glass-epoxy beam elements, the lateral stability enhances significantly by increasing the metal volume fraction. The opposite of this trend can be seen in the case of the carbon-epoxy cross-section.
- For GLARE I-beam, it is seen that the first buckling moment associated with pure bending increases approximately 34% by raising the metal volume percentage from 0% to 20%.
- It can be stated that the effect of changing the percentage of metal on the thickness of both flanges is more pronounced than the one related to the web.
- Regarding to the presented results, it is detected that carbon-epoxy members with different volume fractions always and exposed to different end moment ratio have more lateral stability resistance than glass-epoxy ones.

References

[1] M. Mohammadi, A. Rastgoo, Primary and secondary resonance analysis of FG/lipid nanoplate with considering porosity distribution based on a nonlinear elastic medium, *Mechanics of Advanced Materials and Structures,* Vol. 27, No. 20, pp. 1709-1730, 2020.

[2] M. Mohammadi, M. Hosseini, M. Shishesaz, A. Hadi, A. Rastgoo, Primary and secondary resonance analysis of porous functionally graded nanobeam resting on a nonlinear foundation subjected to mechanical and electrical loads, *European Journal of Mechanics - A/Solids,* Vol. 77, pp. 103793, 2019/09/01/, 2019.

[3] M. Mohammadi, A. Rastgoo, Nonlinear vibration analysis of the viscoelastic composite nanoplate with three directionally imperfect porous FG core, *Structural Engineering and Mechanics, An Int'l Journal,* Vol. 69, No. 2, pp. 131-143, 2019.

[4] A. Farajpour, A. Rastgoo, M. Mohammadi, Vibration, buckling and smart control of microtubules using piezoelectric nanoshells under electric voltage in thermal environment, *Physica B: Condensed Matter,* Vol. 509, pp. 100-114, 2017.

[5] M. Goodarzi, M. Mohammadi, M. Khooran, F. Saadi, Thermo-mechanical vibration analysis of FG circular and annular nanoplate based on the visco-pasternak foundation, *Journal of Solid Mechanics,* Vol. 8, No. 4, pp. 788-805, 2016.

[6] M. Baghani, M. Mohammadi, A. Farajpour, Dynamic and Stability Analysis of the Rotating Nanobeam in a Nonuniform Magnetic Field Considering the Surface Energy, *International Journal of Applied Mechanics,* Vol. 08, No. 04, pp. 1650048, 2016.

[7] M. R. Farajpour, A. Rastgoo, A. Farajpour, M. Mohammadi, Vibration of piezoelectric nanofilm-based electromechanical sensors via higher-order non-local strain gradient theory, *Micro & Nano Letters,* Vol. 11, No. 6, pp. 302-307, 2016.

[8] A. Farajpour, M. Yazdi, A. Rastgoo, M. Mohammadi, A higher-order nonlocal strain gradient plate model for buckling of orthotropic nanoplates in thermal environment, *Acta Mechanica,* Vol. 227, No. 7, pp. 1849-1867, 2016.

[9] A. Farajpour, M. H. Yazdi, A. Rastgoo, M. Loghmani, M. Mohammadi, Nonlocal nonlinear plate model for large amplitude vibration of magneto-electro-elastic nanoplates, *Composite Structures,* Vol. 140, pp. 323-336, 2016.

[10] M. Mohammadi, M. Safarabadi, A. Rastgoo, A. Farajpour, Hygro-mechanical vibration analysis of a rotating viscoelastic nanobeam embedded in a visco-Pasternak elastic medium and in a nonlinear thermal environment, *Acta Mechanica,* Vol. 227, No. 8, pp. 2207-2232, 2016.

[11] M. Safarabadi, M. Mohammadi, A. Farajpour, M. Goodarzi, Effect of surface energy on the vibration analysis of rotating nanobeam, 2015.

[12] H. Asemi, S. Asemi, A. Farajpour, M. Mohammadi, Nanoscale mass detection based on vibrating piezoelectric ultrathin films under thermo-electro-mechanical loads, *Physica E: Low-dimensional Systems and Nanostructures,* Vol. 68, pp. 112-122, 2015.

[13] M. Mohammadi, A. Farajpour, M. Goodarzi, H. Shehni nezhad pour, Numerical study of the effect of shear in-plane load on the vibration analysis of graphene sheet embedded in an elastic medium, *Computational Materials Science,* Vol. 82, pp. 510-520, 2014/02/01/, 2014.

[14] A. Farajpour, A. Rastgoo, M. Mohammadi, Surface effects on the mechanical characteristics of microtubule networks in living cells, *Mechanics Research Communications,* Vol. 57, pp. 18-26, 2014.

[15] M. GOODARZI, M. MOHAMMADI, A. FARAJPOUR, M. KHOORAN, INVESTIGATION OF THE EFFECT OF PRE-STRESSED ON VIBRATION FREQUENCY OF RECTANGULAR NANOPLATE BASED ON A VISCO-PASTERNAK FOUNDATION, *JOURNAL OF SOLID MECHANICS,* Vol. 6, No. 1, pp. -, 2014.

[16] S. Asemi, A. Farajpour, H. Asemi, M. Mohammadi, Influence of initial stress on the vibration of double-piezoelectric-nanoplate systems with various boundary conditions using DQM, *Physica E: Low-dimensional Systems and Nanostructures,* Vol. 63, pp. 169-179, 2014.

[17] S. Asemi, A. Farajpour, M. Mohammadi, Nonlinear vibration analysis of piezoelectric nanoelectromechanical resonators based on nonlocal elasticity theory, *Composite Structures,* Vol. 116, pp. 703-712, 2014.

[18] M. Mohammadi, A. Farajpour, A. Moradi, M. Ghayour, Shear buckling of orthotropic rectangular graphene sheet embedded in an elastic medium in thermal environment, *Composites Part B: Engineering,* Vol. 56, pp. 629-637, 2014.

[19] S. R. Asemi, M. Mohammadi, A. Farajpour, A study on the nonlinear stability of orthotropic single-layered graphene sheet based on nonlocal elasticity theory, *Latin American Journal of Solids and Structures,* Vol. 11, No. 9, pp. 1515-1540, 2014.

[20] M. Mohammadi, A. Farajpour, M. Goodarzi, F. Dinari, Thermo-mechanical vibration analysis of annular and circular graphene sheet embedded in an elastic medium, *Latin American Journal of Solids and Structures,* Vol. 11, pp. 659-682, 2014.

[21] M. Mohammadi, A. Moradi, M. Ghayour, A. Farajpour, Exact solution for thermo-mechanical vibration of orthotropic mono-layer graphene sheet embedded in an elastic medium, *Latin American Journal of Solids and Structures,* Vol. 11, No. 3, pp. 437-458, 2014.

[22] M. Mohammadi, A. Farajpour, M. Goodarzi, H. Mohammadi, Temperature Effect on Vibration Analysis of Annular Graphene Sheet Embedded on Visco-Pasternak Foundati, *Journal of Solid Mechanics,* Vol. 5, No. 3, pp. 305-323, 2013.

[23] M. Mohammadi, A. Farajpour, M. Goodarzi, R. Heydarshenas, Levy type solution for nonlocal thermo-mechanical vibration of orthotropic mono-layer graphene sheet embedded in an elastic medium, *Journal of Solid Mechanics,* Vol. 5, No. 2, pp. 116-132, 2013.

[24] M. Mohammadi, M. Goodarzi, M. Ghayour, A. Farajpour, Influence of in-plane pre-load on the vibration frequency of circular graphene sheet via nonlocal continuum theory, *Composites Part B: Engineering,* Vol. 51, pp. 121-129, 2013.

[25] M. Mohammadi, M. Ghayour, A. Farajpour, Free transverse vibration analysis of circular and annular graphene sheets with various boundary conditions using the nonlocal continuum plate model, *Composites Part B: Engineering,* Vol. 45, No. 1, pp. 32-42, 2013.

[26] M. MOHAMMADI, M. GOODARZI, M. GHAYOUR, S. ALIVAND, SMALL SCALE EFFECT ON THE VIBRATION OF ORTHOTROPIC PLATES EMBEDDED IN AN ELASTIC MEDIUM AND UNDER BIAXIAL IN-PLANE PRE-LOAD VIA NONLOCAL ELASTICITY THEORY, *JOURNAL OF SOLID MECHANICS,* Vol. 4, No. 2, pp. -, 2012.

[27] M. Danesh, A. Farajpour, M. Mohammadi, Axial vibration analysis of a tapered nanorod based on nonlocal elasticity theory and differential quadrature method, *Mechanics Research Communications,* Vol. 39, No. 1, pp. 23-27, 2012.

[28] A. Farajpour, A. Shahidi, M. Mohammadi, M. Mahzoon, Buckling of orthotropic micro/nanoscale plates under linearly varying in-plane load via nonlocal continuum mechanics, *Composite Structures,* Vol. 94, No. 5, pp. 1605-1615, 2012.

[29] M. Mohammadi, M. Goodarzi, M. Ghayour, S. Alivand, Small scale effect on the vibration of orthotropic plates embedded in an elastic medium and under biaxial in-plane pre-load via nonlocal elasticity theory, 2012.

[30] N. GHAYOUR, A. SEDAGHAT, M. MOHAMMADI, WAVE PROPAGATION APPROACH TO FLUID FILLED SUBMERGED VISCO-ELASTIC FINITE CYLINDRICAL SHELLS, *JOURNAL OF AEROSPACE SCIENCE AND TECHNOLOGY (JAST),* Vol. 8, No. 1, pp. -, 2011.

[31] H. Moosavi, M. Mohammadi, A. Farajpour, S. H. Shahidi, Vibration analysis of nanorings using nonlocal continuum mechanics and shear deformable ring theory, *Physica E: Low-dimensional Systems and Nanostructures,* Vol. 44, No. 1, pp. 135-140, 2011/10/01/, 2011.

[32] A. Farajpour, M. Danesh, M. Mohammadi, Buckling analysis of variable thickness nanoplates using nonlocal continuum mechanics, *Physica E: Low-dimensional Systems and Nanostructures,* Vol. 44, No. 3, pp. 719-727, 2011.

[33] A. Farajpour, M. Mohammadi, A. Shahidi, M. Mahzoon, Axisymmetric buckling of the circular graphene sheets with the nonlocal continuum plate model, *Physica E: Low-dimensional Systems and Nanostructures,* Vol. 43, No. 10, pp. 1820-1825, 2011.

[34] M. Mohammadi, M. Ghayour, A. Farajpour, Analysis of Free Vibration Sector Plate Based on Elastic Medium by using New Version of Differential Quadrature Method, *Journal of Simulation and Analysis of Novel Technologies in Mechanical Engineering,* Vol. 3, No. 2, pp. 47-56, 2010.

[35] Y. Xu, J. Zhu, Z. Wu, Y. Cao, Y. Zhao, W. Zhang, A review on the design of laminated composite structures: constant and variable stiffness design and topology optimization, *Advanced Composites and Hybrid Materials,* Vol. 1, No. 3, pp. 460-477, 2018.

[36] A. Muc, P. Kędziora, A. Stawiarski, Buckling enhancement of laminated composite structures partially covered by piezoelectric actuators, *European Journal of Mechanics-A/Solids,* Vol. 73, pp. 112-125, 2019.

[37] A. Elkaimbillah, B. Braikat, F. Mohri, N. Damil, A one-dimensional model for computing forced nonlinear vibration of thin-walled composite beams with open variable cross-sections, *Thin-Walled Structures,* Vol. 159, pp. 107211, 2021.

[38] C. Li, X. Tian, T. He, New insights on piezoelectric thermoelastic coupling and transient thermo-electromechanical responses of multi-layered piezoelectric laminated composite structure, *European Journal of Mechanics-A/Solids,* Vol. 91, pp. 104416, 2022.

[39] M. Soltani, R. Abolghasemian, M. Shafieirad, Z. Abbasi, A. A. Mehra, A. Ghasemi, Multi-objective optimization of lateral stability strength of transversely loaded laminated composite beams with varying I-section, *Journal of Composite Materials,* Vol. 56, No. 12, pp. 1921-1939, 2022.

[40] M. Goodarzi, M. Mohammadi, A. Farajpour, M. Khooran, Investigation of the effect of pre-stressed on vibration frequency of rectangular nanoplate based on a visco-Pasternak foundation, 2014.

[41] S. Rajasekaran, K. Nalinaa, Stability and vibration analysis of non-prismatic thin-walled composite spatial members of generic section, *International Journal of Structural Stability and Dynamics,* Vol. 5, No. 04, pp. 489-520, 2005.

[42] S. P. Machado, V. H. Cortínez, Free vibration of thin-walled composite beams with static initial stresses and deformations, *Engineering Structures,* Vol. 29, No. 3, pp. 372-382, 2007.

[43] T. P. Vo, J. Lee, Flexural–torsional coupled vibration and buckling of thin-walled open section composite beams using shear-deformable beam theory, *International Journal of Mechanical Sciences,* Vol. 51, No. 9-10, pp. 631-641, 2009.

[44] C. Karaagac, H. Ozturk, M. Sabuncu, Effects of an edge crack on the free vibration and lateral buckling of a cantilever laminated composite slender beam, *Journal of Vibration and Control,* Vol. 19, No. 16, pp. 2506-2522, 2013.

[45] L. Ascione, V. P. Berardi, A. Giordano, S. Spadea, Local buckling behavior of FRP thin-walled beams: a mechanical model, *Composite Structures,* Vol. 98, pp. 111-120, 2013.

[46] A. Ghasemi, M. Mohandes, Nonlinear free vibration of laminated composite Euler-Bernoulli beams based on finite strain using generalized differential quadrature method, *Mechanics of Advanced Materials and Structures,* Vol. 24, No. 11, pp. 917-923, 2017.

[47] M. Mohandes, A. R. Ghasemi, Modified couple stress theory and finite strain assumption for nonlinear free vibration and bending of micro/nanolaminated composite Euler–Bernoulli beam under thermal loading, *Proceedings of the Institution of Mechanical Engineers, Part C: Journal of Mechanical Engineering Science,* Vol. 231, No. 21, pp. 4044-4056, 2017.

[48] A. R. Ghasemi, M. Mohandes, A new approach for determination of interlaminar normal/shear stresses in micro and nano laminated composite beams, *Advances in Structural Engineering,* Vol. 22, No. 10, pp. 2334-2344, 2019.

[49] A. R. Ghasemi, M. Heidari-Rarani, B. Heidari-Sheibani, A. Tabatabaeian, Free transverse vibration analysis of laminated composite beams with arbitrary number of concentrated masses, *Archive of Applied Mechanics,* Vol. 91, No. 6, pp. 2393-2402, 2021.

[50] A. Asadi, A. H. Sheikh, O. T. Thomsen, Buckling behaviour of thin-walled laminated composite beams having open and closed sections subjected to axial and end moment loading, *Thin-Walled Structures,* Vol. 141, pp. 85-96, 2019/08/01/, 2019.

[51] !!! INVALID CITATION !!! [50-53].

[52] A. M. M. Bidgoli, M. Heidari-Rarani, Axial buckling response of fiber metal laminate circular cylindrical shells, *Structural Engineering and Mechanics,* Vol. 57, No. 1, pp. 45-63, 2016.

[53] A. R. Ghasemi, M. Mohandes, Comparison between the frequencies of FML and composite cylindrical shells using beam modal function model, *Journal of Computational Applied Mechanics*, Vol. 50, No. 2, pp. 239-245, 2019.

[54] A. R. Ghasemi, S. Kiani, A. Tabatabaeian, Buckling analysis of FML cylindrical shells under combined axial and torsional loading, *Mechanics of Advanced Composite Structures*, Vol. 7, No. 2, pp. 263-270, 2020.

[55] A. R. Ghasemi, M. Mohandes, Free vibration analysis of micro and nano fiber-metal laminates circular cylindrical shells based on modified couple stress theory, *Mechanics of Advanced Materials and Structures*, Vol. 27, No. 1, pp. 43-54, 2020.

[56] R. Syah, D. Ramdan, M. Elveny, M. Mohandes, A. Khan, A. Nouri, A. B. Albadarin, Computational simulation of critical speed and dynamic analysis of agglomerated CNTs/fiber/polymer/metal laminates rotating cylindrical shell, *Arabian Journal of Chemistry*, Vol. 14, No. 10, pp. 103358, 2021.

[57] G. S. Dhaliwal, G. M. Newaz, Compression after impact characteristics of carbon fiber reinforced aluminum laminates, *Composite Structures*, Vol. 160, pp. 1212-1224, 2017.

[58] M. Mohandes, A. R. Ghasemi, M. Irani-Rahagi, K. Torabi, F. Taheri-Behrooz, Development of beam modal function for free vibration analysis of FML circular cylindrical shells, *Journal of Vibration and Control*, Vol. 24, No. 14, pp. 3026-3035, 2018.

[59] R. J. Mania, Z. Kolakowski, J. Bienias, P. Jakubczak, K. Majerski, Comparative study of FML profiles buckling and postbuckling behaviour under axial loading, *Composite Structures*, Vol. 134, pp. 216-225, 2015.

[60] D. Banat, R. Mania, Stability and strength analysis of thin-walled GLARE composite profiles subjected to axial loading, *Composite Structures*, Vol. 212, pp. 338-345, 2019.

[61] D. Banat, R. Mania, R. Degenhardt, Stress state failure analysis of thin-walled GLARE composite members subjected to axial loading in the post-buckling range, *Composite Structures*, Vol. 289, pp. 115468, 2022.

[62] V. Z. Vlasov, Thin-walled elastic beams, *PST Catalogue*, Vol. 428, 1959.

[63] J. Lee, S.-E. Kim, K. Hong, Lateral buckling of I-section composite beams, *Engineering Structures*, Vol. 24, No. 7, pp. 955-964, 2002.

[64] R. Bellman, J. Casti, Differential quadrature and long-term integration, *Journal of mathematical analysis and Applications*, Vol. 34, No. 2, pp. 235-238, 1971.

[65] C. W. Bert, M. Malik, Differential quadrature method in computational mechanics: a review, 1996.

[66] V. ANSYS, 5.4, Swanson Analysis System, Inc, 2007.

[67] M. Soltani, A Novel Approach for Lateral Buckling Assessment of Double Tapered Thin-Walled Laminated Composite I-Beams, *Mechanics of Advanced Composite Structures*, Vol. 9, No. 1, pp. 11-23, 2022.

[68] M. Soltani, F. Atoufi, Non-local finite element formulation for stability analysis of thin-walled nanobeams with varying I-section, *Acta Mechanica*, Vol. 233, No. 2, pp. 789-811, 2022.